Quaternary Research (2022), **106**, 147–161
doi:10.1017/qua.2021.60

Research Article

Chronology, time averaging, and oxygen isotope composition of harvested marine mollusk assemblages from Ifri Oudadane, northeast Morocco

William Sanchez[a], Yurena Yanes[a]*, Jörg Linstädter[b] and Rainer Hutterer[c]

[a]Department of Geology, University of Cincinnati, Cincinnati Ohio 45221, USA; [b]Deutsches Archäologisches Institut, Kommission für Archäologie Außereuropäischer Kulturen (KAAK), Bonn, Germany and [c]Zoologisches Forschungsmuseum Alexander Koenig, 53113 Bonn, Germany

Abstract

The archaeological site of Ifri Oudadane, NE Morocco, contains well-preserved marine mollusk concentrations throughout the Epipaleolithic (hunting-gathering) and Neolithic (food production) cultural phases, useful to test hypotheses driving such transition. However, the chronology and stratigraphy of harvested shells is complex due to the confluence of human activity and natural deposition processes. This work first quantifies the age and degree of time averaging of archaeological shells and then estimates sea-surface temperatures (SSTs) from the oxygen isotopes of selected specimens. Thirty-four radiocarbon-dated shells exhibited significant time averaging between 310 to 1170 yr that could not be explained by analytical error alone. This finding illustrates the need for individually dating shells in future paleoclimate investigations aiming for high temporal resolution. Nine isotopically analyzed shells dated to the Neolithic phase, between 5700 and 7600 cal yr BP, indicate that assuming constant oxygen isotopes of seawater, SSTs remained consistently warm, between 20°C and 22°C, that is, 2°C–4°C warmer than today. Results point to warmer conditions during the Neolithic, supporting the hypothesis that the rise of a food production mode of life in NE Morocco could have in part been triggered by warming conditions following the colder 8.2 event.

Keywords: *Phorcus turbinatus*, Carbonate-target radiocarbon dating, Age mixing, Paleothermometry, Archaeological record, Holocene, NW Africa

(Received 26 May 2021; accepted 7 September 2021)

INTRODUCTION

Harvested mollusk assemblages are frequently preserved in coastal and island environments and have been used to infer past subsistence strategies, resource manipulation, and paleoenvironmental and paleoecological conditions (e.g., Mannino et al., 2007, 2008; Colonese et al., 2009; Andrus, 2011; Prendergast et al., 2013, 2016). Shells are often preserved in so-called middens, which can be defined as ancient human garbage dumps with high concentrations of discarded foods (e.g., shells) and other remains accumulated throughout time. However, the study of archaeological shell concentrations can be challenging, because an array of natural and anthropogenic processes are involved in the formation of middens, and these processes are difficult to disentangle (Parker et al., 2020).

To properly interpret the stratigraphy and geochronology of mollusk shell assemblages, it is essential to quantify the scale of time averaging, or the mixing of remains of different ages occurring in the same stratigraphic layer (Kidwell and Bosence, 1991; Kowalewski, 1996; New et al., 2019; Parker et al., 2020). Failing to recognize time averaging can lead to the misinterpretation of ancient assemblages that may have the appearance of being isochronous while they are actually diachronous (Kidwell and Bosence, 1991; Kowalewski, 1996; New et al., 2019; Parker et al., 2020). There are various natural sedimentary processes that can lead to the mixing of noncontemporaneous remains in the same horizon. Some of these include changes in sedimentation (burial) rates, exhumation and reburial of older material, taphonomic pressures (decay rates), and mixing due to biological activity (Fürsich and Aberhan, 1990; Kidwell and Bosence, 1991; Kowalewski, 1996; Parker et al., 2020). In archaeological settings, anthropogenic factors can contribute to time averaging, including pit digging, trampling, and so on, which may lead to additional complexities when interpreting the environmental context of mollusk assemblages (Koppel et al., 2016; Parker et al., 2020).

The Mediterranean region is characterized by a long history of human occupation, and many of these coastal settlements have left an accessible harvested mollusk record, providing an opportunity to investigate human and environmental evolution over multimillennial timescales (Colonese et al., 2011). Archaeological mollusk assemblages have been extensively utilized in the last few decades as a credible tool to reconstruct the paleoclimate and associated human cultural or socioeconomic transitions (e.g., Colonese et al., 2009; Mannino et al., 2007; Prendergast

*Corresponding author: Department of Geology, University of Cincinnati, Cincinnati, Ohio 45221, USA. E-mail address: yurena.yanes@uc.edu (Y. Yanes).

Cite this article: Sanchez W, Yanes Y, Linstädter J, Hutterer R (2022). Chronology, time averaging, and oxygen isotope composition of harvested marine mollusk assemblages from Ifri Oudadane, northeast Morocco. *Quaternary Research* **106**, 147–161. https://doi.org/10.1017/qua.2021.60

et al., 2016; Yanes et al., 2018). The bulk of published work on shell middens has generally assumed that shells retrieved from the same horizon or close stratigraphic position were collected at equivalent times and therefore lump them together in the same age group. This hypothesis seems reasonable and is based on stratigraphic and archaeological evidence. Intriguingly, some recent studies (e.g., Koppel et al., 2016; Parker et al., 2020) have documented that in some cases, shell middens may exhibit multicentennial to multimillennial time averaging that cannot be detected based on stratigraphic position alone, reinforcing the complexity in geochronology and stratigraphy of harvested mollusk concentrations. The scarce number of studies that have examined the scale of time averaging in shell middens is in part explained because traditional graphite-target radiocarbon dating is rather costly and tedious. Recently, Bush et al. (2013) developed a new method, the carbonate-target radiocarbon dating method, which can be conducted at a much lower cost and more rapidly than the traditional graphite-target radiocarbon dating. Accordingly, we now have the logistic ability to measure the degree of time averaging in archaeological shelly accumulations by individually dating numerous shells retrieved from the same stratigraphic layer.

In NE Morocco, the coastal archaeological site of Ifri Oudadane embraces a Holocene record from 5700 to 11,000 cal yr BP that preserves the cultural transition from hunter-gatherers to a food production mode of life (Linstädter and Kehl, 2012; Morales et al., 2013). The site also contains rich concentrations of edible-size marine mollusk *Phorcus turbinatus*, as early humans incorporated marine resources into their diets through the practice of foraging throughout all cultural periods (Linstädter and Kehl, 2012; Hutterer et al., 2014; Yanes et al., 2018). The scientific community has proposed several hypotheses to explain the reasons behind this shift, including increases in population density, decrease in prey due to excessive hunting, and climate and environmental change among others (Weisdorf, 2005). The shells preserved throughout the stratigraphy at Ifri Oudadane offer an excellent opportunity to reconstruct paleoclimatic conditions during part of the Holocene in NE Morocco. This is because mollusk shells grow in a continuous accretionary fashion, and the oxygen isotope composition ($\delta^{18}O$) of the calcium carbonate can be used to infer the temperature during calcification if the water $\delta^{18}O$ value is inferred independently or assumed to have a constant value (Grossman and Ku, 1986).

In this study, we use the carbonate-target radiocarbon dating approach to date numerous shells of the harvested marine gastropod *P. turbinatus* from the Ifri Oudadane site in NE Morocco to test the hypothesis that shells preserved jointly in the same cultural phase are indeed contemporaneous and exhibit minimal time averaging. This study assesses the structure (age distribution) and scale (range of age) of time averaging of harvested shells at the site. The dated shells are then calibrated to calendar age and those ages are compared with the calibrated ages of previously dated terrestrial archaeological remains in the site using the graphite-target radiocarbon method. Additionally, potential radiocarbon age differences between outer and inner aragonitic layers of the same shell are examined to test for potential radiocarbon offsets between shell layers. Finally, selected radiocarbon-dated shells were used to reconstruct submonthly Holocene sea-surface temperature (SST) data derived from oxygen isotope time-series analyses to test the hypothesis that the rise of food production in NW Africa coincides with climate and environmental change. This work illustrates the potential impacts of not sampling individual shells, which should be considered in future paleoclimatic and archaeological inferences using human-harvested mollusk concentrations.

MATERIAL AND METHODS

Geographic, archaeological, and chronological setting

The archaeological site of Ifri Oudadane (Fig. 1a and b), located in NE Morocco (35.2151°N, 3.2543°W), is a coastal marble cliff rock shelter that is ~5 m high and ~15 m wide and is positioned ~50 m above the present-day shoreline (Linstädter and Kehl, 2012). This site was discovered in 2006 during roadwork, and since then, a number of excavations during the years 2006, 2007, 2010, and 2011 have retrieved archaeological remains (Linstädter and Kehl, 2012). The rock shelter itself formed as a result of high stand in sea level that ultimately exposed the rock and led to erosion generating the cavity of the cave (Linstädter and Kehl, 2012). The region is part of the Rif range, where there is active plate collision occurring that is likely the cause for sea level to be ~50 m below the present cavity of the cave (Michard et al., 2008).

In previous studies, the chronology at Ifri Oudadane has been constrained from a total of 25 published radiocarbon dates from archaeological plant and vertebrate remains (Table 1), which suggests that the occupational period at the site spans from ~11,000 to ~5700 cal yr BP, which can be divided into two main cultural periods, the Epipaleolithic (EPI) and the Early Neolithic (EN) (Fig. 1c) (Linstädter and Kehl, 2012; Morales et al., 2013, 2016; Linstädter et al., 2016). The transition from the Epipaleolithic to the Early Neolithic can be distinguished by changes in manufacturing, decoration, and form present in pottery as well as the appearance of domesticated plants and animals (Linstädter and Kehl, 2012; Morales et al., 2013; Linstädter et al., 2015). The Early Neolithic phase is further subdivided into the Early Neolithic A (ENA), Early Neolithic B (ENB), and Early Neolithic C (ENC) (Fig. 1c). For the previously published radiocarbon dates there were 6 dates for the EPI layer, 5 for ENA, and 15 for ENB (Linstädter and Kehl, 2012; Morales et al., 2013; Linstädter et al., 2015). The Epipaleolithic (~7600 to ~11,000 cal yr BP) represents the hunting-gathering society before the transition to Neolithic innovations and food production (Zapata et al., 2013; Linstädter and Kehl 2012). The Epipaleolithic layer exhibits ~100 cm of thickness and contains bones of wild animals as well as sparse lithic tools (Linstädter et al., 2015). The Neolithic layers are 1.5 m thick and contain ash lenses and charcoal, impressed pottery, and domesticated plants and animals (Morales et al., 2013). The oldest subdivision of the EN layer is the ENA, which spans from ~7000 to ~7600 cal yr BP (Linstädter and Kehl, 2012). The ENA layer is an ~20 cm thick layer that contains cardium-decorated pottery and domesticated ovicaprines (Linstädter and Kehl, 2012). The first domesticated crops appear in the ENA layer, which is the Epipaleolithic–Early Neolithic boundary, defined by a lentil dated to 7611 ± 37 cal yr BP (Morales et al., 2013). The dated lentil is also the oldest evidence of food production in all of North Africa (Morales et al., 2013). The ENB subdivision spans from ~6700 to ~7000 cal yr BP and is considered the main occupational period at Ifri Oudadane (Linstädter and Kehl, 2012). Variations in pottery can be seen between the ENA and the ENB (Linstädter and Kehl, 2012). The final subdivision is the ENC, spanning ~6300 to ~6600 cal yr BP. Late Neolithic deposits of Ifri Oudadane are not represented by a proper layer. One charcoal sample yielded a radiocarbon age of 5763 ± 80 cal yr BP (KIA 39296), which is consistent with the timing of the Late Neolithic phase in this site (Linstädter, 2008).

Since its discovery, Ifri Oudadane has been the focus of numerous studies over the past decade. Linstädter and Kehl

https://doi.org/10.1017/qua.2021.60 Published online by Cambridge University Press

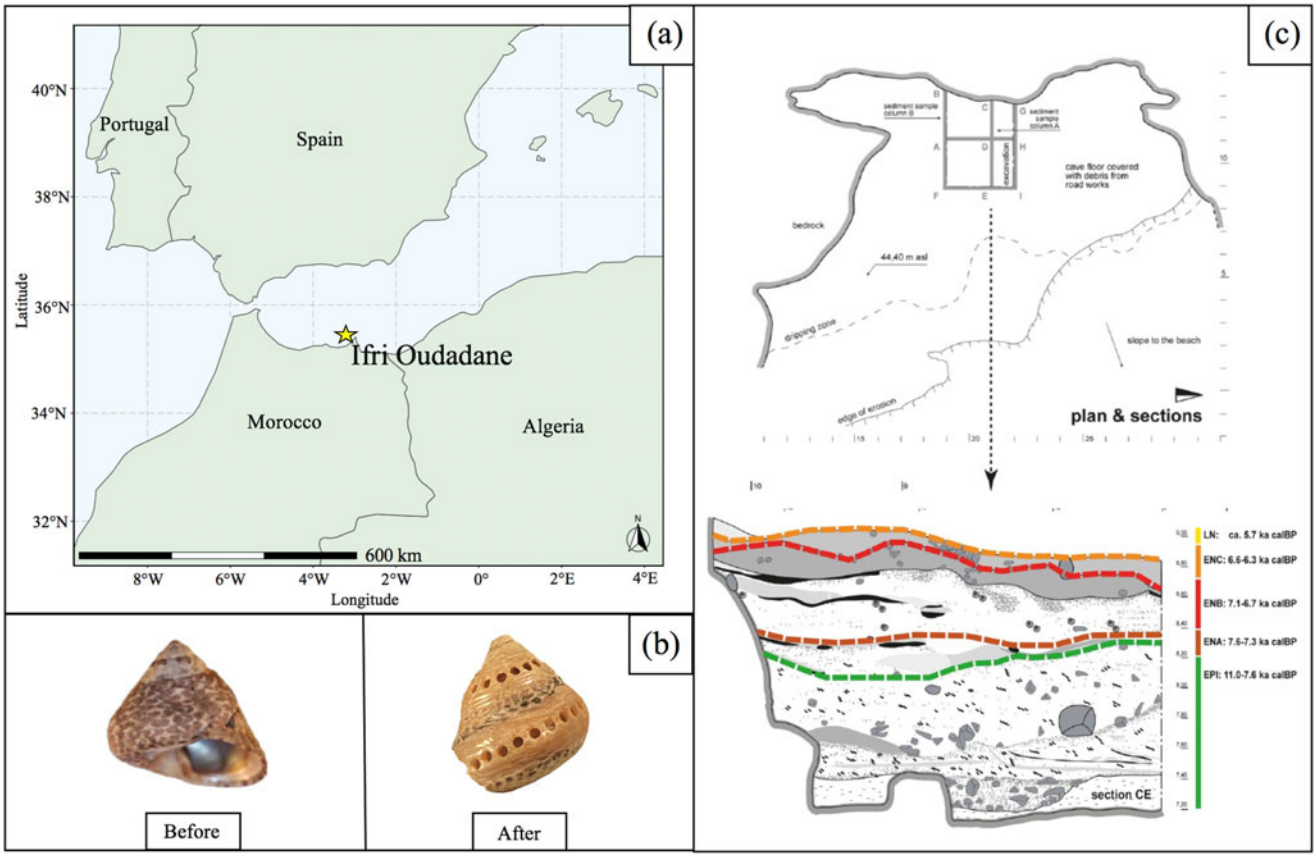

Figure 1. (a) Geographic location of Ifri Oudadane, NE Morocco. (b) Photograph of an archaeological *Phorcus turbinatus* shell from Ifri Oudadane. The shells are shown before and after sequential drilling for time-series isotopic analysis. (c) Schematic of the stratigraphy from Ifri Oudadane with the chronology for each cultural period from previously published radiocarbon dates (adopted from Yanes et al. 2018).

(2012) defined the archaeological sequence and examined the processes that may have formed the site. The presence of coprolites and calcite spherulites in the Early Neolithic layer reflect the penning of domesticated animals in the cave. Linstädter and Wagner (2013) examined the pottery preserved throughout the stratigraphy to further define the cultural transition from the Epipaleolithic to the Neolithic by observing changes in manufacturing, decoration, and form in pottery remains. Zapata et al. (2013) studied the paleobotanical evidence to deduce how ancient human populations utilized their surroundings as well as if and how the environment changed throughout the occupational phase at Ifri Oudadane. Linstädter et al. (2015) examined the lithic industry that was present at the site. Yanes et al. (2018) investigated the season of shellfish harvest and noticed the apparent link between climate change and cultural transition by analyzing three shells. Finally, Hutterer et al. (2021) analyzed the shellfish remains at the site to determine the usage of shellfish in diet; examine the temporal change in shellfish size; and assess the usage of shellfish for tools and ornaments.

Current climate, vegetation, and oceanographic conditions

In the present day, the climate in NE Morocco is Mediterranean type, with wet and mild winters, arid and hot summers, and a wet season between fall and spring (Morales et al., 2013). The vegetation in the area today is a maquia-type forest, which includes junipers (*Juniperus* sp.), pines (*Pinus* sp.), wild olive (*Olea* europaea), and Holm oaks (*Quercus ilex*) (Morales et al., 2013). Ifri Oudadane's surroundings have been subjected to depletion of natural resources and deforestation in the last few decades (Morales et al., 2013).

Ifri Oudadane is positioned on the coast of the westernmost portion of the Alboran Sea, which is connected to the Atlantic Ocean via the Strait of Gibraltar. Dense saline water from the Alboran Sea exits through the Strait of Gibraltar into the Atlantic Ocean, whereas less-dense water with lower salinity from the Atlantic enters the Mediterranean (Pierre, 1999; Bazzicalupo et al., 2018). The inflow of the water with lower salinity from the Atlantic creates two gyres in the Alboran Sea (Pierre, 1999; Bazzicalupo et al., 2018). Ifri Oudadane is situated near the westernmost gyre of the Alboran Sea. Shaltout and Omstedt (2014) reported SSTs from the Alboran Sea between 1982 and 2012 and observed that, on average, the annual SST, winter SST, spring SST, summer SST, and autumn SST were 18.6°C, 15.5°C, 18.0°C, 22.8°C, and 18.8°C, respectively.

The present environmental conditions at Ifri Oudadane and northwest Africa are dictated by several climate mechanisms, including the Intertropical Convergence Zone (ITCZ), the westerly winds, and the North Atlantic Oscillation (NAO) (Bazzicalupo et al., 2018; Padgett et al., 2019). The seasonal migration of the ITCZ affects wind intensity in the area as well as the African monsoon rain (Bazzicalupo et al., 2018). The westerly winds bring rainfall to northern Africa during the winter months (Bazzicalupo et al., 2018). The sea level pressure

https://doi.org/10.1017/qua.2021.60 Published online by Cambridge University Press

Table 1. Previously published graphite-target radiocarbon results (n = 25) from terrestrial plant and vertebrate remains retrieved from Ifri Oudadane site by Linstädter and Kehl (2012), Morales et al. (2013, 2016), and Linstädter et al. (2016).

Ref. laboratory	Other ID	Cultural phase	Material	Species	^{14}C age yr BP	2σ cal yr BP	Median age	Ref.[a]
KIA 39296	Pos. 116	LN	Charcoal	*Juniperus communis*	5000 ± 30	5651–5887	5725	1
Beta 295772	Pos. 487	ENC	Cereal	Emmer wheat	5590 ± 40	6299–6442	6365	1
Beta 295777	Pos. 764	ENC	Cereal	Barley	5670 ± 40	6322–6558	6452	1
Erl 9987	Pos. 11	ENC	Charcoal	*Juniperus communis*	5756 ± 49	6441–6666	6556	1
Erl 9988	Pos. 31	ENB	Charcoal	*Juniperus communis*	6175 ± 50	6945–7240	7077	1
Erl 9989	Pos. 42	ENB	Charcoal	*Olea* sp.	6053 ± 50	6749–7152	6906	1
Beta 295773	Pos. 520	ENB	Cereal	Barley	5980 ± 40	6721–6936	6819	1
Beta 295774	Pos. 537	ENB	Cereal	Barley	5980 ± 40	6721–6936	6819	1
KIA 39298	Pos. 274	ENB	Charcoal	*Juniperus communis*	6085 ± 25	6882–7144	6948	1
KIA 39297	Pos. 258	ENB	Charcoal	*Juniperus communis*	6155 ± 30	6965–7161	7068	1
Beta 295775	Pos. 635	ENB	Cereal	Indeterminate wheat	5910 ± 40	6651–6846	6730	1
Beta 295776	Pos. 678	ENB	Cereal	Emmer wheat	5900 ± 40	6639–6841	6720	1
Beta 295778	Pos. 766	ENB	Pulse	Pea	5930 ± 40	6664–6877	6754	1
Oxa 23528	Pos. 354	ENB	Bone	*Capra hircus*	6136 ± 34	6942–7159	7039	1
KIA 39299	Pos. 343	ENA	Charcoal	*Juniperus communis*	6400 ± 90	7158–7498	7327	1
Beta 295779	Pos. 860	ENA	Pulse	Lentil	6740 ± 50	7511–7677	7604	1
Erl 12419	Pos. 381	EPI	Bone	*Sus scrofa*	7451 ± 56	8177–8377	8273	1
Erl 12418	Pos. 352	EPI	Bone	*Ammotragus lervia*	9496 ± 183	10,293–11,221	10805	1
KIA 39299/2	Pos. 343	ENA	humid acid	*Juniperus communis*	6615 ± 30	7441–7567	7507	1
Beta 313468	Pos. 989	EPI	Dwarf palm	*Chamaeorops humilis*	8080 ± 40	8781–9127	9012	2
Beta 313467	Pos. 945	EPI	Dwarf palm	*Chamaeorops humilis*	7150 ± 40	7872–8029	7973	2
Beta 316137	Pos. 890	EPI	Dwarf palm	*Chamaeorops humilis*	6780 ± 40	7577–7678	7629	2
Beta 318608	Pos. 835	ENA	Wheat	*Triticum* sp.	6140 ± 30	6951–7157	7049	2
Beta 313469	Pos. 1398	EPI	Charcoal		7990 ± 40	8662–9005	8868	3
Beta 341129	Pos. 1368	ENA	Pea	*Pisum sativum*	6160 ± 30	6972–7162	7072	4

[a]Ref.: 1, Linstädter and Kehl, 2002; 2, Morales et al., 2013; 3, Linstädter et al. 2016; 4, Morales et al., 2016.

gradient from Iceland to Azores, characterized by the NAO index, causes variations in storm intensity and the westerly winds (NOAA, 2012; Bazzicalupo et al., 2018; Padgett et al., 2019). The mode of the NAO switches between positive and negative according to variations of pressure at sea level between the Azores high-pressure system and the Icelandic low-pressure system (NOAA, 2012; Parker et al., 2020). A high pressure difference between the Azores high-pressure system and the Icelandic low-pressure system results in a positive mode of NAO, leading to increased westerly winds and storms over northern Europe and Scandinavia. In contrast, a low-pressure difference between the Azores high-pressure system and the Icelandic low-pressure system results in a negative mode of NAO, leading to decreased westerly winds and storms over southern Europe and North Africa (NOAA, 2012).

Radiocarbon dating of marine shells

The new carbonate-target radiocarbon dating method was chosen to date a high number of shells because it is rapid and more cost-effective compared with the traditional graphite-target radiocarbon dating. The carbonate-target radiocarbon dating is approximately one-third the cost of traditional graphite-target radiocarbon dating. Moreover, for samples that are younger than 10,000 yr old, this method yields statistically indistinguishable results compared with the traditional graphite-target method (Bush et al., 2013; Parker et al., 2020; Bright et al., 2021). To test the potential radiocarbon offsets within different layers of the same shell, three shells were selected to assess whether or not the outer and inner aragonitic portion of the same shell would yield statistically equivalent radiocarbon ages. In addition, a total of 34 archaeological *P. turbinatus* shells were individually dated to measure the scale (age range) and structure (age-frequency distribution) of time averaging.

Carbonate-target radiocarbon analyses were conducted at the W.M. Keck Carbon Cycle Accelerator Mass Spectrometer facility at the University of California, Irvine. For the analysis, 0.3 mg of cleaned shell material was ground into a fine powder; mixed with 5 mg of unbaked Alfa Aesar no. 40510, −325 mesh, 99.99% pure Nb; poured into the aluminum cathode target; and pressed for accelerator mass spectrometry measurement (Bush et al., 2013).

https://doi.org/10.1017/qua.2021.60 Published online by Cambridge University Press

Samples originating from a marine environment require an additional correction before they can be directly compared with terrestrial samples. Deep-ocean waters are isolated from the atmosphere, and with time their ^{14}C content is depleted by radioactive decay with respect to the atmosphere (Stuiver and Braziunas, 1993). The deep-ocean water eventually rises to the surface, and marine organisms end up capturing a ^{14}C signal that is depleted with respect to the atmosphere. This process results in marine samples appearing to be older than contemporaneous terrestrial samples, which is known as the marine reservoir carbon effect (Stuiver and Braziunas, 1993). Moreover, due to the complexity and spatial variability in oceanic circulation patterns, the reservoir effect can vary significantly from region to region. The regional offset from the average global marine reservoir correction is defined as (ΔR) (Stuiver and Braziunas, 1993).

Radiocarbon ages were calibrated using CALIB 8.2 (Stuiver et al., 2021) and the marine calibration curve Marine20 with a calculated ΔR (Stuiver and Braziunas, 1993; Heaton et al., 2020). Using the Marine Reservoir Correction Database from CALIB 8.2, sites (n = 6) were selected throughout the Mediterranean from Siani et al. (2000) and Reimer and McCormac (2002) to determine the ΔR (Stuiver et al., 2021). The weighted mean ΔR was calculated based on the uncertainty in each data point (Bevington, 1969). The weighted mean ΔR and the associated uncertainty used for the correction were determined to be −89 ± 78. Based on Stuiver and Polach (1977), the samples were corrected for ^{13}C fractionation. Calibrated radiocarbon ages are reported using a 2σ range in age, which provides a 95.4% probability that the ages fall within this range.

The uncalibrated radiocarbon ages of marine shells were used when evaluating the degree and structure of age mixing, because we are not interested in the actual age, but the age offsets, following previous procedures (Yanes et al., 2007; Kowalewski et al., 2018; Parker et al., 2020). Radiocarbon ages were corrected for ΔR and calibrated to calendar years when comparing our results with previously published radiocarbon ages of terrestrial samples and when shells were used to infer SSTs (see additional justifications in the following sections).

Radiocarbon results are reported in years before present (yr BP), where 0 = 1950 CE. Uncalibrated radiocarbon ages are presented as "^{14}C yr BP," whereas calibrated radiocarbon ages are reported as "cal yr BP".

Measuring the scale and structure of time averaging

To investigate the scale (age range) and structure (age-frequency distribution) of time averaging, we used uncalibrated rather than calibrated radiocarbon ages. Our goal here is to assess age offsets, ranges, and distributions of shell assemblages rather than establishing a calendar age. Because the calibration of radiocarbon ages to calendar years introduces errors, this part of the study was performed using uncalibrated ages only, following previously published work (Yanes et al. 2007; Kowalewski et al. 2018; Parker et al. 2020).

Time averaging needs to be evaluated relative to the variability in shell age that would be expected based on the uncertainty that is associated with radiocarbon dating alone. This can be evaluated by a simple Monte Carlo simulation for each cultural period (Yanes et al., 2007; Parker et al., 2020). The Monte Carlo simulation is used to define the scale of "artificial" time averaging, that is, what you would expect if all the shells were the exact same age, or effectively no time averaging. The Monte Carlo simulation estimates the apparent time averaging derived by uncertainty associated with radiocarbon dating imprecisions alone. This can then be compared with the observed range of radiocarbon values in each assemblage analyzed. The Monte Carlo simulation was carried out using the R statistical programming environment (R Core Team, 2013). In each of the Monte Carlo simulations, a number of values equal to the number of radiocarbon-dated specimens per cultural period (ENA = 4, ENB = 13, EPI = 17) were drawn at random from a normal distribution. The normal distribution for the simulation is equal to the mean radiocarbon age of the cultural period with a standard deviation that has been empirically derived to be 80 yr, which corresponds with the average observed analytical error. Next, the standard deviation was calculated from the randomly drawn values, and this process was conducted iteratively 10,000 times. This resulted in a distribution of standard deviations from 10,000 randomly selected values from a normal distribution. The assumption that errors should be normally distributed is reasonable, because errors associated with radiocarbon dating are expected to be distributed this way (Yanes et al. 2007). In addition, according to the central limit theorem, when multiple sources of error are averaged, the combined errors will be normally distributed (Yanes et al. 2007). Thereafter, the 95th percentile for the distribution of standard deviations was calculated. If the actual standard deviation for the cultural period exceeds the 95th percentile that was identified in the Monte Carlo simulation, this would indicate that the standard deviation in the cultural period should be greater than what would be expected based on analytical uncertainties, such as laboratory imprecision. Accordingly, radiocarbon ages from individuals in the same assemblage would indeed show real time averaging.

The age-frequency distribution or structure of time averaging was evaluated by constructing histograms with 50-yr bins of the uncalibrated radiocarbon ages of individually dated shells from each of the cultural phases (Fig. 2). The scale of time averaging was determined by measuring the range of ages for each of the cultural periods.

Selection of shells for isotopic analyses and time-series sampling protocol

Mollusk assemblages were field collected during the 2011 excavation of Ifri Oudadane, and shells were shipped to the University of Cincinnati, where they were cleaned and prepped. Nine radiocarbon-dated archaeological shells were selected for sequential isotopic sampling along ontogeny to calculate SST at the time of a cultural transition in NE Morocco. Four shells were selected from the EPI phase, two from the ENA phase, and three from the ENB phase. Shells were first mechanically cleaned with tap water and a soft-bristle brush and then placed into a J.P. Selecta Ultrasonic bath for ∼5 min to ensure that any remaining dirt was removed. This process was repeated as needed, after which the shells were left to dry for 24 h at room temperature.

Shells were sampled following standard procedures using archaeological *P. turbinatus* shells (Mannino et al., 2008; Colonese et al., 2009; Prendergast et al., 2013; Parker et al., 2017; Yanes et al., 2018). First, the outer aragonitic portion of the shell was removed using a Dremel® 4000 variable-speed rotary tool with a grinding attachment. Then, the inner aragonitic layer was sampled using a Dremel® 4000 variable-speed rotary tool with a 0.6 mm cutting attachment. Calcium carbonate aliquots were sampled sequentially in ∼1 mm increments from the shell margin, which corresponds to the time of death, up the whirl along

https://doi.org/10.1017/qua.2021.60 Published online by Cambridge University Press

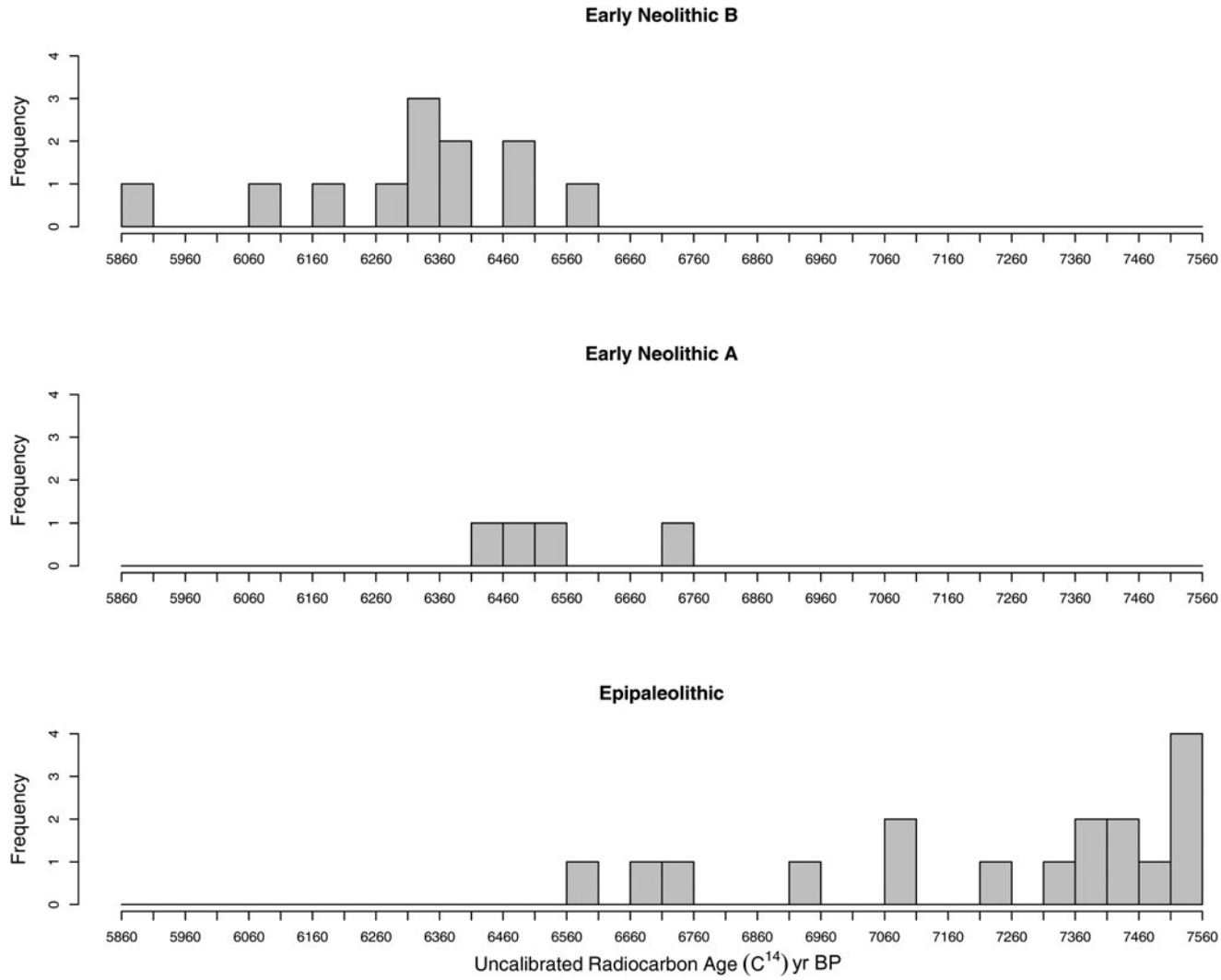

Figure 2. Histograms of age-frequency distributions for uncalibrated radiocarbon ages of archaeological *Phorcus turbinatus* shells. Each histogram depicts one of the three cultural periods (Epipaleolithic, Early Neolithic A, Early Neolithic B) present at Ifri Oudadane, NE Morocco. Histogram bin size = 50 yr.

the growth direction, which depicts the earlier life of the organisms (Fig. 1b). About 30 carbonate aliquots were extracted from each shell, which then were isotopically analyzed.

Oxygen stable isotopic analyses

Calcium carbonate (aragonite) aliquots were analyzed for oxygen isotopic composition at the Light Stable Isotope Mass Spectrometry Laboratory in the Department of Geological Sciences at the University of Florida. Samples were analyzed using a Finnigan-MAT 252 Isotope Ratio Mass Spectrometer coupled with a Kiel III automated carbonate preparation device. Approximately 40–50 mg of carbonate powder from each archaeological shell was digested in 100% H_3PO_4 (specific gravity = 1.92) at 70°C for 10 min, and the CO_2 gas was mass analyzed. Results from the analysis are reported in standard delta notation ($\delta^{18}O$) relative to Vienna Pee Dee Belemnite (VPDB) where values are reported in standard per mil notation:

$$\delta^{18}O = [(^{18}O/^{16}O_{sample}/^{18}O/^{16}O_{standard})-1] \quad \text{(Eq. 1)}$$

Analytical precision was± 0.2‰ (2σ), based on repeated measurements of isotope standards NBS-19 ($\delta^{18}O = -2.20$‰ VPDB) and NBS-18 ($\delta^{18}O = -23.01$‰ VPDB) throughout runs.

Paleotemperature calculations

The measured $\delta^{18}O$ values from archaeological shells were used to calculate SST at the time the biogenic carbonate precipitated using the following equation:

$$SST\ (^{\circ}C) = 20.6-4.34*[(\delta^{18}O_{shell})-(\delta^{18}O_{seawater}-0.27)] \quad \text{(Eq. 2)}$$

This equation was first proposed by Grossman and Ku (1986), but it contains an additional correction by Dettman et al. (1999) for the conversion from Vienna Standard Mean Ocean Water (VSMOW) to VPDB. Each sampled shell yielded ~30 carbonate aliquots capturing the last year of the organism's life span.

The oxygen isotope composition ($\delta^{18}O$) of the surface seawater for the westernmost portion of the Alboran Sea has been measured by Pierre (1999). Based on five measurements, Pierre (1999) determined that average surface seawater $\delta^{18}O$ value was

https://doi.org/10.1017/qua.2021.60 Published online by Cambridge University Press

+1.0‰ (VSMOW), ranging from +0.7‰ to +1.2‰. Thus, annual/seasonal variation in oxygen isotope values of seawater in the Mediterranean are up to ~0.5‰ (see also Prendergast et al., 2013). Martrat et al. (2007) used multiple proxies (forams, alkenones, etc.) from a deep-sea core that suggested that $\delta^{18}O$ values of seawater remained relatively constant throughout the Holocene in the western Alboran Sea. Based on these studies, we assumed a constant surface seawater $\delta^{18}O$ value of +1.0‰ (VSMOW), and this value was adopted for paleotemperature calculations using equation 2 shown above. The shell $\delta^{18}O$ values have an analytical precision of ± 0.2‰ (2σ) which is similar to ±0.6°C error in the SST calculations. In a recent publication, Mette et al. (2018) showed that isotope records derived from single shells are not sufficient to provide robust estimates of proxy error. In addition, potential errors derived from seawater oxygen isotope variability should be considered (Prendergast et al., 2013). Taking these additional errors into account, the SST estimates presented here should exhibit a greater error up to ±1°C (Prendergast et al., 2013).

Finally, the degree of seasonality recorded in each measured shell was then calculated from the difference of the coldest and warmest temperature registered by each individual during its last year of growth. As demonstrated in Wanamaker et al. (2011), the amplitude of seasonality from shells should be calculated considering the same number of samples of the last year of growth to minimize biases in these estimates. In our study, the last year of growth was assumed based on the sinusoidal cycles in the isotope values of each shell and equivalent sampling resolution.

RESULTS

Radiocarbon ages of archaeological shells

Previously published radiocarbon ages are summarized in Table 1, whereas new radiocarbon dates from this work are summarized in Tables 2 and 3. The uncalibrated radiocarbon results of inner and outer aragonitic layers retrieved from the same shell resulted in statistically equal ages for EPI1 and EPI3. Interestingly, shell EPI2 showed inner and outer aragonitic ages with an ~200 yr offset (Table 3). Uncalibrated radiocarbon ages of dated shells ranged in age from ~586 ^{14}C yr BP for an Early Neolithic B shell (ENB1) to ~7560 ^{14}C yr BP for an Epipaleolithic shell (EPI17) (Tables 2 and 4).

After the marine reservoir effect correction and calibration of results to calendar years for comparison with other terrestrial remains that were dated by published work (see Table 5), the shells ranged in age from ~5580 to ~8190 cal yr BP.

Scale and structure of time averaging

To assess the scale (age range) and structure (age-frequency distribution) of time averaging, 13 and 20 shells were individually dated for the cultural periods ENB and EPI, respectively. Only four shells were dated for the ENA phase, because it is the thinnest layer, only ~20 cm thick, with lower abundance of shells. Uncalibrated radiocarbon ages for each cultural period (ENB, ENA, and EPI) are reported in Table 4. The shell assemblages exhibited multicentennial time averaging ranging from 310 to 1170 ^{14}C yr BP (Table 4). Shell assemblages from the ENB phase showed ages from 5860 to 6600 ^{14}C yr BP, that is, a total range of 740 yr. The mollusk assemblage from the ENA phase varied in age from 6440 to 6750 ^{14}C yr BP, with a total age range of 310 yr. Finally, the shell assemblage from the EPI phase displayed minimum and maximum ages of 6390 and 7560 ^{14}C yr BP, respectively, which results in an age range of 1170 yr. In Figure 2, age-frequency histograms show the structure of time averaging for each of the cultural periods separately.

The Monte Carlo 95th percentile results were 102.8, 128.2, and 106.4 for EPI, ENA, and ENB, respectively (Table 4). In all cases, the standard deviation exceeded the Monte Carlo 95th percentile, which suggests that the age ranges of these samples are beyond analytical error associated with radiocarbon dating.

Oxygen isotopes and SST calculations

Oxygen isotopes and SST calculations results are summarized in Table 6. The nine shells that were selected for time-series isotopic analysis ranged in age from 6170 to 7930 cal yr BP. Calibrated radiocarbon ages are used here because our goal is to infer SSTs during calendar years and for comparison with other work. Figure 3 shows the submonthly $\delta^{18}O$ values for each shell separately. Across all cultural periods, the $\delta^{18}O$ values from the shells ranged from −0.4 ± 0.2‰ to 1.8 ± 0.3‰. The mean shell $\delta^{18}O$ value of all analyzed shells was 0.5 ± 0.2‰. In Figure 4, the average $\delta^{18}O$ values (n = ~30) per shell are plotted against calibrated radiocarbon ages to assess how $\delta^{18}O$ values have varied throughout time.

Figure 5 illustrates the calculated SSTs from each shell. The shells indicate that SSTs during the Early–Middle Holocene in NE Morocco varied from 15.9 ± 1.4°C to 25.6 ± 0.9°C.When all archaeological shells are combined, the average SST was 21.3 ± 0.8°C, that is, ~3°C warmer than today, on average. The average observed SST per shell can be plotted against calibrated radiocarbon ages to depict how SST has varied throughout time (Fig. 6).

Submonthly SST time series per shell illustrate that measured specimens appear to have grown shell during summer and winter seasons. The magnitude of seasonality registered in each shell ranged from 8.3°C to 11.9°C, averaging 9.7 ± 1.3°C (Fig. 5, Table 6). This value is consistent with present-day amplitude of seasonality.

Shell ENB4 yielded the warmest mean annual temperature (~22.5°C), corresponding to the Early Neolithic B period, while shell EPI6 yielded the coolest mean annual temperature (~19.8°C), corresponding to the Epipaleolithic period (Figs. 5 and 6).

DISCUSSION

Time averaging of harvested marine mollusk shells

Based on the 34 radiocarbon-dated shells from the Ifri Oudadane archaeological site, we argue that some seemingly contemporaneous mollusk shells exhibit multicentennial time averaging beyond analytical error that ranged from 310 to 1170 yr. The scale of time averaging in archaeological settings is driven by multiple sedimentary and human processes operating simultaneously (Parker et al., 2020). For example, several studies have shown that low sedimentation rate leads to an increase in time averaging (e.g., Fürsich and Aberhan, 1990; Kidwell and Bosence, 1991; Kowalewski, 1996; Kidwell, 1998; Parker et al., 2020), which is the most plausible scenario for the sediment succession at the rock shelter of Ifri Oudadane. Moreover, the human utilization of the site by deposition of archaeological material and year-round occupancy is likely to lead to increased time averaging. Indeed, Yanes et al. (2018) showed that Ifri Oudadane was occupied year-round, which points

https://doi.org/10.1017/qua.2021.60 Published online by Cambridge University Press

Table 2. New carbonate-target radiocarbon results from 34 Holocene harvested *Phorcus turbinatus* marine shells from the Ifri Oudadane site.

Ref. laboratory	Other ID	Cultural phase	Material	Species	Age ^{14}C yr BP	2σ cal yr BP	Median age
ENB6	Pos.1070	ENB	Marine gastropod	*Phorcus turbinatus*	6070 ± 60	6160–6660	6400
ENB7	Pos.1070	ENB	Marine gastropod	*Phorcus turbinatus*	6380 ± 60	6460–7010	6740
ENB8	Pos.1070	ENB	Marine gastropod	*Phorcus turbinatus*	6510 ± 60	6620–7160	6890
ENB9	Pos.1070	ENB	Marine gastropod	*Phorcus turbinatus*	6350 ± 60	6430–6970	6700
ENB10	Pos.1095	ENB	Marine gastropod	*Phorcus turbinatus*	6470 ± 70	6570–7140	6840
ENB11	Pos.1095	ENB	Marine gastropod	*Phorcus turbinatus*	6290 ± 60	6370–6910	6630
ENB12	Pos.1095	ENB	Marine gastropod	*Phorcus turbinatus*	6340 ± 70	6410–6970	6690
ENB13	Pos.1095	ENB	Marine gastropod	*Phorcus turbinatus*	6020 ± 70	6080–6630	6340
ENB4	Pos.1170	ENB	Marine gastropod	*Phorcus turbinatus*	6330 ± 110	6340–7020	6680
ENB3	Pos.1176	ENB	Marine gastropod	*Phorcus turbinatus*	6400 ± 100	6440–7100	6760
ENB1	Pos.1177	ENB	Marine gastropod	*Phorcus turbinatus*	5860 ± 90	5880–6460	6170
ENB2	Pos.1213	ENB	Marine gastropod	*Phorcus turbinatus*	6600 ± 110	6650–7300	6990
ENB5	Pos.1260	ENB	Marine gastropod	*Phorcus turbinatus*	6190 ± 120	6200–6880	6530
ENA4	Pos.1322	ENA	Marine gastropod	*Phorcus turbinatus*	6490 ± 100	6530–7180	6860
ENA2	Pos.1357	ENA	Marine gastropod	*Phorcus turbinatus*	6750 ± 110	6810–7430	7140
ENA1	Pos.1399	ENA	Marine gastropod	*Phorcus turbinatus*	6560 ± 100	6630–7250	6940
ENA3	Pos.1403	ENA	Marine gastropod	*Phorcus turbinatus*	6440 ± 100	6490–7140	6807
EPI3	Pos.1455	EPI	Marine gastropod	*Phorcus turbinatus*	6960 ± 110	7050–7630	7350
EPI2	Pos.1457	EPI	Marine gastropod	*Phorcus turbinatus*	6700 ± 110	6770–7400	7090
EPI4	Pos.1459	EPI	Marine gastropod	*Phorcus turbinatus*	7080 ± 120	7160–7760	7470
EPI5	Pos.1491	EPI	Marine gastropod	*Phorcus turbinatus*	6590 ± 100	6650–7270	6980
EPI1	Pos.1515	EPI	Marine gastropod	*Phorcus turbinatus*	6720 ± 120	6770–7420	7110
EPI10	Pos.1639	EPI	Marine gastropod	*Phorcus turbinatus*	7410 ± 80	7530–8020	7780
EPI11	Pos.1639	EPI	Marine gastropod	*Phorcus turbinatus*	7450 ± 80	7560–8070	7820
EPI12	Pos.1639	EPI	Marine gastropod	*Phorcus turbinatus*	7550 ± 80	7660–8180	7920
EPI13	Pos.1639	EPI	Marine gastropod	*Phorcus turbinatus*	7380 ± 80	7510–7990	7750
EPI14	Pos.1639	EPI	Marine gastropod	*Phorcus turbinatus*	7560 ± 80	7660–8190	7930
EPI15	Pos.1639	EPI	Marine gastropod	*Phorcus turbinatus*	7460 ± 80	7570–8080	7830
EPI6	Pos.1640	EPI	Marine gastropod	*Phorcus turbinatus*	7240 ± 70	7390–7860	7620
EPI7	Pos.1640	EPI	Marine gastropod	*Phorcus turbinatus*	7080 ± 80	7220–7710	7470
EPI8	Pos.1640	EPI	Marine gastropod	*Phorcus turbinatus*	7520 ± 80	7630–8160	7890
EPI9	Pos.1640	EPI	Marine gastropod	*Phorcus turbinatus*	7500 ± 80	7610–8140	7870
EPI16	Pos.1640	EPI	Marine gastropod	*Phorcus turbinatus*	7360 ± 80	7490–7970	7730
EPI17	Pos.1640	EPI	Marine gastropod	*Phorcus turbinatus*	7560 ± 80	7660–8190	7930

to frequent input rate of shells leading to larger time averaging. Koppel et al. (2016) showed that postdepositional anthropogenic disturbances can also lead to an increase in time averaging. In the case of Ifri Oudadane, Linstädter and Kehl (2012) documented that some shells likely were trampled and reworked on the cave floor by either humans or animals before the shells were buried by sediments and sealed. Human trampling, building of fireplaces, digging of pits, and animal scavenging activities, among others, are likely to have occurred in the site, leading to some shell reworking postdeposition. The results presented here are consistent with some other studies on shell middens. For example, Parker et al. (2020) dated numerous harvested mollusk shells from middens present at various sites in the Canary Islands and documented a multicentennial scale of time averaging in some cases in which remains that appeared to be contemporaneous actually were of different ages. Koppel et al. (2016) examined shell middens with rich concentrations of charcoal and bivalves in northwest Australia, and their analyses demonstrated significant time averaging as well. All these studies and the present work emphasize that archaeological shell concentrations may exhibit multicentennial time averaging and

https://doi.org/10.1017/qua.2021.60 Published online by Cambridge University Press

Table 3. Carbonate-target uncalibrated radiocarbon dates of pure aragonite samples derived from the inner and outer portions of the same shell.

Ref. laboratory	Age (^{14}C yr BP)
EPI1-outer	6700 ± 100
EPI1-inner	6720 ± 120
EPI2-outer	6390 ± 110
EPI2-inner	6700 ± 110
EPI3-outer	6910 ± 110
EPI3-inner	6960 ± 110

call for precautions when examining the ages of these type of deposits.

While the Early Neolithic A layer has too small of a sample size (n = 4) to assess the age-frequency distribution of shells, a sufficient sample size was accessible for the Epipaleolithic (n = 17) and Early Neolithic B (n = 13) phases. In terms of the structure, or age-frequency distribution of the uncalibrated radiocarbon ages, both cultural phases showed a marked left-skewed distribution, that is, older age shells were more prominent, while the younger shells became less common (Fig. 2). In contrast, the majority of published studies on natural marine shelly assemblages have noted a consistent right-skewed distribution (e.g., Kowalewski et al., 1998; Kidwell et al., 2005), which indicates that younger shells are more prevalent in the stratigraphy, whereas the oldest shells are increasingly less abundant due to more prominent decay associated with longer residence time in the taphonomic (destructive) active zone. This taphonomic model does not seem to apply to the archaeological mollusk assemblages investigated here, suggesting that other processes rather than taphonomic decay are impacting these shell concentrations. Left-skewed age-frequency distribution of shelly accumulations could be explained by the human or animal footprint during site occupation at Ifri Oudadane. For example, humans and/or animals could bury slightly younger shells into older layers or depths in the profile without clear stratigraphic evidence of the process, resulting in a left-skewed age-frequency distribution.

The empirical data from the ENA phase at Ifri Oudadane have been critically debated, as they depict the oldest evidence for food and pottery production in the region. Zilhão (2014) argues that the definitive breakthrough of cereal cultivation in southern Spain and the region of Tangier, Morocco, did not occur until 200–300 yr later than the date documented at Ifri Oudadane. Furthermore, Zilhão (2014) questions that in loose sediments such as an "escargotière" (i.e., snail shell midden), age mixing is likely and therefore fine-stratigraphic studies would be impossible without a substantial number of radiocarbon dates. The results presented here seem to support Zilhão's (2014) point. Archaeological investigations of shell middens in general, and especially those focusing on the transition to food production, must therefore continue carefully in this region. Nevertheless, the archaeological record of Ifri Oudadane remains as a powerful and accessible piece of prehistory to further investigate the timing and reasons behind the rise of food production in the area.

It is important to review some of the assumptions and parameters that are made in the Monte Carlo simulation (Table 4). In all cultural phases, the actual standard deviations of the samples exceed the 95th percentile value of the 10,000 simulated Monte Carlo draws. It should be kept in mind that this is based on a calculation error of 80 for the standard deviation for all of the Monte Carlo draws. However, the ENA set of samples appears to have a calculation error higher than 80. With that being said, if a calculation error of 100 was used, the standard deviation of the ENA set would likely not exceed the Monte Carlo 95th percentile value. However, the other two sets of samples from the ENB and EPI phases have statistically larger standard deviations, and they would continue to exceed the Monte Carlo 95th percentile value, even when considering a greater analytical error of 100 yr.

Calibrated radiocarbon ages of archaeological shells were compared with published ages from Ifri Oudadane derived from terrestrial plant and vertebrate remains (Linstädter and Kehl 2012; Morales et al. 2013, 2016; Linstädter et al. 2016; Table 5). The new calibrated radiocarbon ages in this study from marine shells were mostly consistent with previously dated terrestrial remains. Interestingly, the shells retrieved from the upper Epipaleolithic phase showed slightly younger ages than anticipated. This incongruency calls for caution when assigning the age of an archaeological layer from ages derived merely from harvested shells, because processes like trampling, digging, and scavenging could potentially distort the stratigraphic position of shells (Koppel et al., 2016; Parker et al., 2020).

In this study, we dated the inner and outer aragonite layers of the same shell separately, using the carbonate-target radiocarbon method (Table 3). Our study showed that the inner and outer aragonite from the same shell yielded statistically equivalent age results in two out of the three shells that were dated. However, in EPI2, the inner and outer aragonite showed an ~200 yr offset between the layers. This observed ~200 yr offset may be explained by diagenetic alteration of the outer layer. High temperatures derived from cooking or burning activities (>300°C) may cause significant changes in the geochemistry of the shell (Milano et al., 2016, 2018). However, the shells analyzed here did not show visual evidence of heat exposure, and further research is needed to evaluate the potential effects of diagenetic alteration in radiocarbon results. This work illustrates that the rapid and more affordable carbonate-target radiocarbon method proved to be a valid and reliable tool for calculating the age of Holocene archaeological shells, in agreement with previous studies testing the validity of the method and successfully applying it (e.g., Kowalewski et al., 2018; New et al., 2019; Parker et al., 2020; Bright et al., 2021).

Paleotemperature inferences from archaeological shells

The $\delta^{18}O$ values along shell growth direction suggest that the analyzed archaeological shells of *P. turbinatus* exhibit submonthly resolution, and the quasi-sinusoidal trend suggests that specimens deposited shell relatively consistently during both winter and summer seasons (Fig. 3). The published literature has shown that about 1 mm of the shell seems to correspond to 2–4 weeks of the organism's life, which shows that *Phorcus* tracks submonthly SST at the sampling resolution employed, in agreement with other studies (e.g., Parker et al., 2017, 2020). Published studies from other regions in the Mediterranean suggest that *Phorcus* grow relatively continuously year-round, but growth rates seem to decrease or stop at SSTs above 25°C (Mannino et al., 2008; Colonese et al., 2009). However, Prendergast et al. (2013) documented that *P. turbinatus* from Malta can grow shell at temperatures of 27°C. Thus, our *P. turbinatus* specimens from Morocco

https://doi.org/10.1017/qua.2021.60 Published online by Cambridge University Press

Table 4. Summary of the uncalibrated radiocarbon ages from mollusk assemblages retrieved from three cultural phases at Ifri Oudadane site, combined with results from the Monte Carlo simulation.

Cultural phase	Number of shells	Min. age (^{14}C yr BP)	Max. age (^{14}C yr BP)	Age range (yr)	Sample mean	Sample SD	Monte Carlo 95th percentile
ENB	13	5860	6600	740	6293	208	106
ENA	4	6440	6750	310	6560	136	128
EPI	20	6390	7560	1170	7242	328	103

Table 5. Summary of the range of radiocarbon calibrated ages for each cultural phase separately (ENB, ENA, EPI) at Ifri Oudadane site from previously published work and the present study combined.

	Published graphite-target ages from terrestrial remains[a]			New carbonate-target ages from marine mollusks		
Cultural phase	Min. age (cal yr BP)	Max. age (cal yr BP)	n	Min. age (cal yr BP)	Max. age (cal yr BP)	n
ENB	6640	7240	10	5880	7300	13
ENA	6970	7680	5	6490	7430	4
EPI	7580	11,220	6	6410	8190	20

[a]Linstädter and Kehl, 2002; Morales et al., 2013, 2016; Linstädter et al. 2016.

likely grew nearly year-round, with the possibility of some underestimation of the hottest parts of the year.

The measured $\delta^{18}O$ values here ranged between -0.4 ± 0.2‰ and $+1.8 \pm 0.3$‰ (Fig. 3, Table 6) and are generally consistent with $\delta^{18}O$ values reported in other studies that have analyzed *P. turbinatus* shells throughout the Mediterranean, which have primarily focused on modern specimens for calibration purposes (Mannino et al., 2008; Prendergast et al., 2013) or on archaeological shells to identify seasons of harvest collection (Mannino et al., 2007; Colonese et al., 2009; Prendergast et al., 2016; Yanes et al., 2018).

Modern SSTs in the Alboran Sea range from 15.5°C in winter to 22.8°C in summer, with an average SST of 18.6 ± 3.0°C (Shaltout and Omstedt, 2014). Calculated SSTs from archaeological *P. turbinatus* shells suggest that SSTs during the Early Neolithic in NE Morocco ranged from 15.9 ± 1.4°C to 25.6 ± 0.9°C, with a mean value of 21.3 ± 0.8°C. The results presented here suggest that winter temperatures seem to have remained relatively consistent to the present; however, summer temperatures seem to have been several degrees warmer than today. Due to warmer summer seasons, the average annual SSTs recorded in the shells are also warmer than modern (last few decades) instrument records. The observed warmer summer seasons between 6170 and 7930 cal yr BP could indicate that climate change occurred during the transition from hunting-gathering activities into a food production mode of life. These findings are consistent with previous evidence that correlated the appearance of domesticated plants in the site with gradually warming conditions (Yanes et al., 2018). The present study shows the apparent importance of warming summer temperatures in promoting prehistoric food production, which could have been a factor contributing to the rise of a food production mode of life in Northwest Africa.

Even though the results from this study from nine archaeological shells suggest a relatively consistent average annual SST from 6170 to 7930 cal yr BP of about 21°C (Fig. 6, Table 6), the coolest mean annual SST was obtained from one of the oldest shells (EPI6), dated to 7620 cal yr BP (19.8°C), whereas the warmest mean annual SST was retrieved from one of the youngest shells (ENB4), dated to 6680 cal yr BP (22.5°C) (Fig. 6, Table 6). Although the number of shells analyzed is not sufficient to draw definite conclusions, this apparent warming trend from the end of the Epipaleolithic into the Early Neolithic B is consistent with trends identified in other independent published proxies in Morocco (Cheddadi et al., 1998) and the Alboran Sea (Cacho et al., 1999; Martart et al., 2007; Bazzicalupo et al., 2020). Martart et al. (2007) examined deep-sea core ODP-977A and noted that alkenone-derived SSTs exhibited a warming trend from ~8200 to ~6800 cal yr BP. Cacho et al. (1999) examined alkenone-derived SSTs from deep-sea core MD952043 and reported a similar warming trend. In a recent publication, Bazzicalupo et al. (2020) studied the deep-sea core for Ocean Drilling Program Site 976 and reconstructed SSTs using planktonic foraminifera. Their results again showed a warming trend following the sudden decease in global temperature that occurred at 8200 cal yr BP, known as the 8.2 event. Their results indicate that the warmest temperatures occurred from 7700 to 5800 cal yr BP, with temperatures up to 23°C during summer and 16°C during winter, values consistent with results from this study.

All in all, the present and several previous paleoclimate studies in the western Mediterranean and NW Africa support a 2 to 3 degree warmer scenario during the Early–Middle Holocene than at present, following the 8.2 event. The fact that the detected warming conditions coincide with the first appearance of domesticated remains in NW Africa supports the hypothesis that warming conditions may have in part triggered the rise of food production in the area (Yanes et al., 2018).

The analyzed shells registered summer and winter temperatures throughout their lifespans (Fig. 5). These results show that the degree of seasonality has remained consistent between 6170 and 7930 cal yr BP, with an SST difference between summer and winter of 9.7 ± 1.3°C, on average. However, the degree of seasonality is slightly larger than what is seen in the modern-day SST instrument records, that is, 7.3°C (Shaltout and Omstedt, 2014), which can be explained by several-degree warmer summers during the Early–Middle Holocene than today (Yanes et al., 2018). It is likely that a combination of factors played a role in the climate variability in the Alboran Sea during the Early–Middle Holocene. Lorenz and Lohmann (2004) suggest that orbital changes in insolation represent one of the primary drivers of SST variability in the Alboran Sea. Català et al. (2019) argue that orbital changes in insolation can only account for ~1.6°C of the 5°C or greater climate variability that is seen throughout

https://doi.org/10.1017/qua.2021.60 Published online by Cambridge University Press

Table 6. Summary of nine archaeological shell $\delta^{18}O$ values and calculated sea-surface temperature (SST) at Ifri Oudadane site.

Ref. laboratory	Median age (cal yr BP)	Sample size	$\delta^{18}O$ ‰ (VPDB)			SST (°C)			
			Min	Max	Mean	Min	Max	Mean	Range
EPI3	7350	31	−0.4	2.4	0.7	13.4	25.3	20.9	11.9
EPI4	7470	31	−0.4	1. 7	0.5	16.5	25.4	21.8	8.8
EPI6	7620	26	−0.3	2.1	0.9	14.8	24.9	19.8	10.1
EPI7	7930	26	−0.3	1.6	0.5	16.8	25.1	21.8	8.3
ENA1	6940	31	−0.9	1.8	0.6	16.1	27.6	21.3	11.5
ENA2	7140	31	−0.3	2.0	0.6	15.0	24.9	21.2	9.9
ENB1	6170	31	−0.4	1.6	0.6	16.9	25.4	21.3	8.5
ENB4	6680	31	−0.7	1.3	0.3	18.1	26.7	22.5	8.6
ENB5	6530	31	−0.3	1.9	0.7	15.6	25.2	20.8	9.6
Means			−0.4	1.8	0.5	15.9	25.6	21.3	9.7
SD (+)			0.2	0.3	0.2	1.4	0.9	0.8	1.3

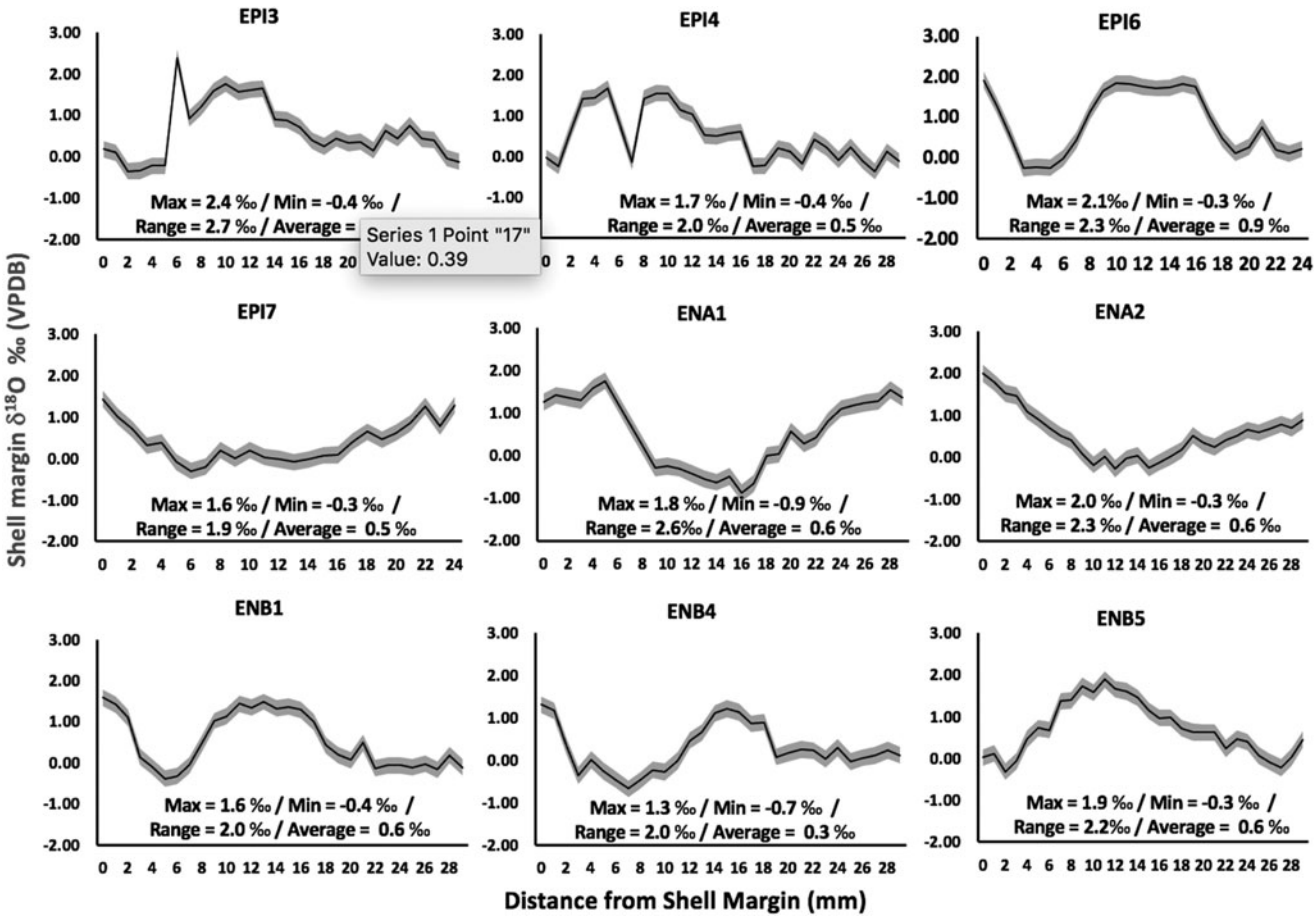

Figure 3. Oxygen isotope values of nine radiocarbon-dated archaeological *Phorcus turbinatus* shells collected from Ifri Oudadane, NE Morocco. The envelopes surrounding the data correspond to an analytical error of ±0.2 ‰ (2σ).

the Holocene. Instead, Català et al. (2019) propose that mixing of water masses through the Straits of Gibraltar impact temperature changes in the area in combination with orbital changes in isolation. The mixing of water masses from the Atlantic Ocean through the Straits of Gibraltar following the 8.2 event or the last deglaciation could have potentially decreased the northward

https://doi.org/10.1017/qua.2021.60 Published online by Cambridge University Press

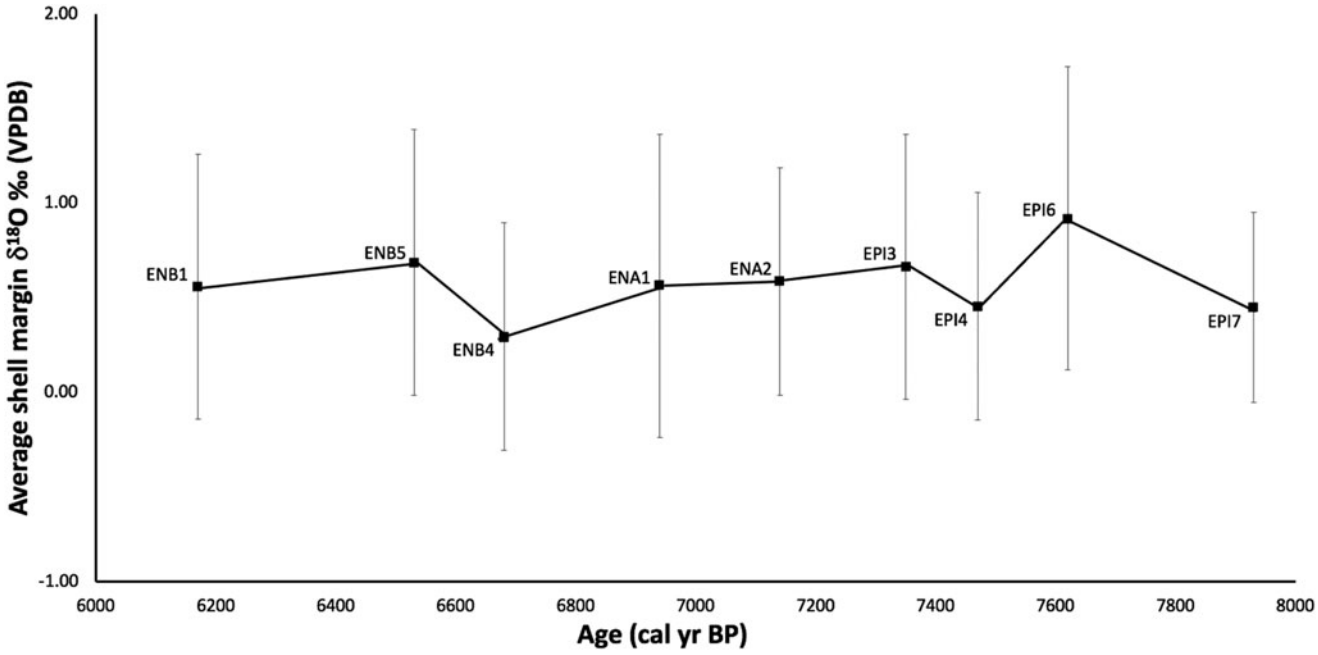

Figure 4. Average observed $\delta^{18}O$ values from nine archaeological *Phorcus turbinatus* shells collected from Ifri Oudadane, NE Morocco, compared with calibrated radiocarbon ages. Error bars represent the standard deviation in observed $\delta^{18}O$ values for each shell.

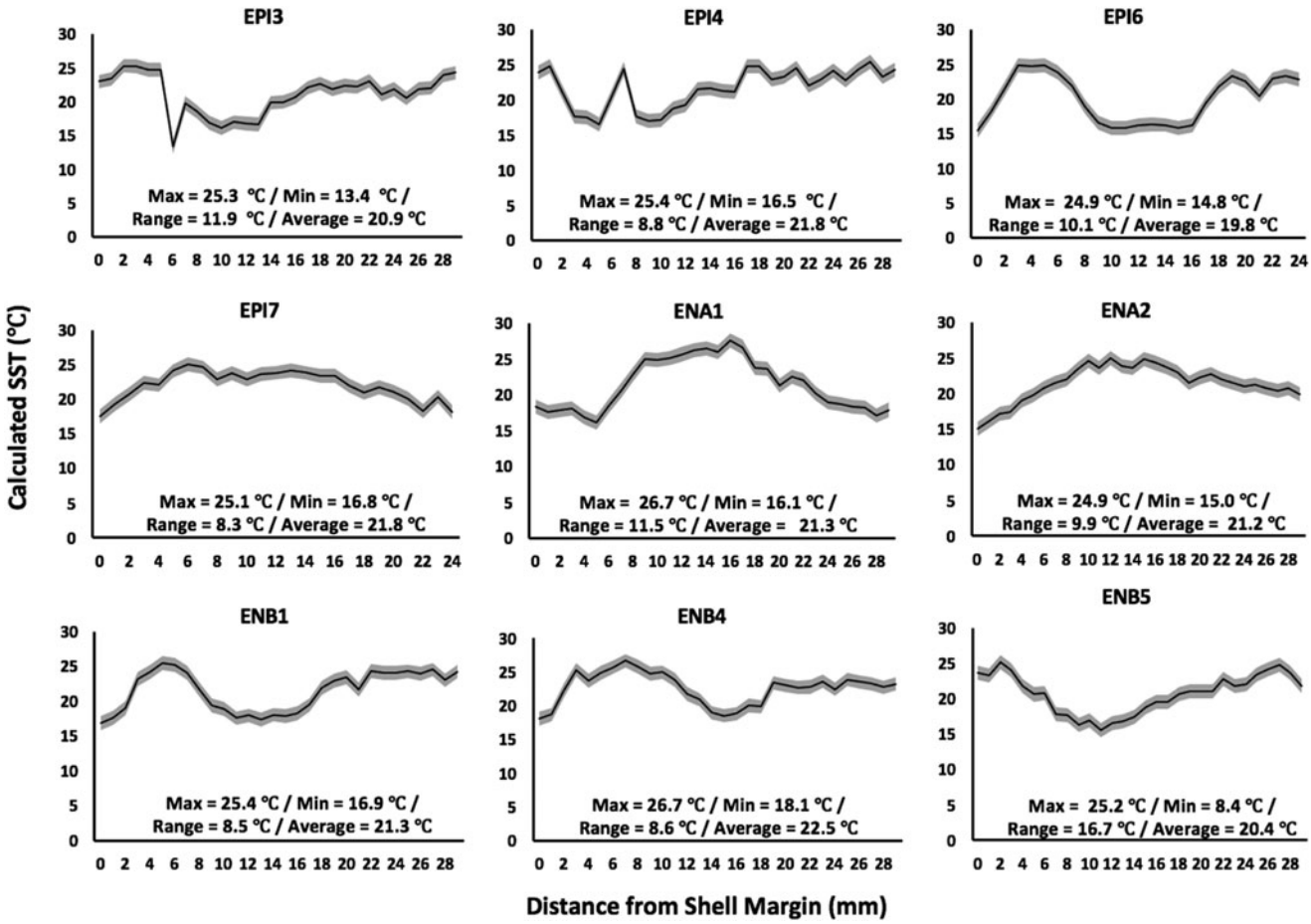

Figure 5. Calculated sea-surface temperatures (SSTs) from nine radiocarbon-dated archaeological *Phorcus turbinatus* shells collected from Ifri Oudadane, NE Morocco. The envelopes surrounding the data correspond to an analytical error of ± 1°C.

https://doi.org/10.1017/qua.2021.60 Published online by Cambridge University Press

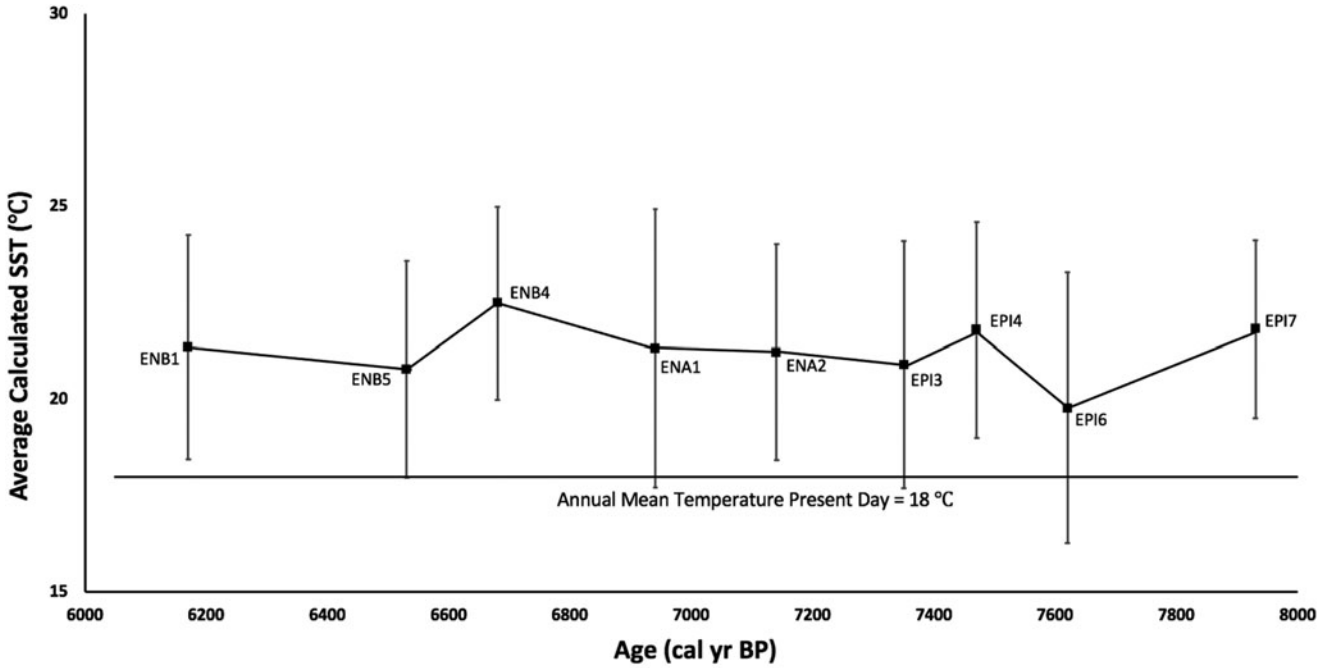

Figure 6. Average annual sea-surface temperatures (SSTs) calculated from the oxygen isotope time series of nine radiocarbon-dated archaeological *Phorcus turbinatus* shells from Ifri Oudadane, NE Morocco. Error bars represent the standard deviations in SST data for each shell. The horizontal line represents the average annual temperature for the present day.

heat transport from the subtropical gyre, leading to an accumulation of heat that eventually entered into the Alboran Sea through the Straits of Gibraltar (Yanes et al., 2018; Català et al., 2019).

CONCLUSIONS

New radiocarbon dates on 34 *P. turbinatus* shells retrieved from the Holocene archaeological succession of Ifri Oudadane, NE Morocco, reveal that these assemblages exhibit multicentennial time averaging beyond analytical error that were unclear by stratigraphic and archaeological position. This is likely due to low sedimentation rates and continuous site occupation by humans and domesticated animals. Interestingly, dated shells showed left-skewed distributions, indicating that older shells were more frequent than younger ones. This finding is in sharp contrast with natural marine shell beds, which consistently show a right-skewed structure in response to faster taphonomic decay of older shells.

This study calls for caution when assuming the age of harvested mollusk assemblages, and we advise individually dating numerous shells when possible. The present work also shows that dating shells alone may not be the best approach to understand the history of site occupation, because shells are too strongly affected by site-formation processes. We propose that directly dating artifacts and other food remains within an archaeological context is probably a more adequate approach to understand site occupation history.

Two out of the three shells tested exhibited indistinguishable ages between the inner and outer aragonite layers. Using this more affordable dating technique, we are able to date numerous specimens at low cost and gain new insights into the genesis and preservation of archaeological mollusk assemblages. Thus, we recommend radiocarbon dating each shell to constrain paleoclimatic information more robustly through time.

While the stratigraphy and chronology of harvested shelly assemblages may be difficult to understand, shells are powerful paleoclimate proxies when they are individually radiocarbon dated for finer chronological control. New oxygen isotope results from nine archaeological shells suggest that SSTs on the coast of NE Morocco during the Early Neolithic (between 6100 and 7600 cal yr BP) were ~2°C to 4°C warmer than at present. This apparently warmer scenario is consistent with the rise of a food production mode of life in NW Morocco, which could indicate a potential link between prehistoric food production and climate change; however, further studies in NW Africa are still needed to confirm this possibility.

Acknowledgments. Special thanks go to John Southon (University of California, Irvine) for assisting with radiocarbon analyses, Jason Curtis (University of Florida) for assisting with oxygen isotope analyses, and Arnie Miller (University of Cincinnati) for assisting with the Monte Carlo simulation. We also thank Abdessalam Mikdad from the Institut National des Sciences de l'Archéologie et du Patrimoine in Rabat, Morocco, and the Deutsches Archäologisches Institut, Bonn, Germany for long-term, amicable cooperative work and for providing site data. Special thanks go to editor Derek Booth, associate editor Louisa Bradtmiller, and reviewers Alan Wanamaker and Amy Prendergast for providing detailed and constructive comments that greatly improved the clarity and quality of this work.

Financial Support. Fieldwork was funded by the German Research Foundation (DFG) in the frame of the CRC 806 "Our Way to Europe." Research with the mollusk samples was partially funded by National Science Foundation (NSF) grant no. 1802153 awarded to Y.Y. Additional support was provided by NSF/GSA Graduate Student Geoscience grant no. 12938-20 to W.S., which is funded by NSF award no. 1949901.

REFERENCES

Andrus, C.F.T., 2011. Shell midden sclerochronology. *Quaternary Science Reviews* **30**, 2892–2905.

Bazzicalupo, P, Maiorano, P, Girone, A, Marino, M., Combourieu-Nebout, N., Incarbona, A. 2018. High-frequency climate fluctuations over the last deglaciation in the Alboran Sea, Western Mediterranean: Evidence from calcareous plankton assemblages. *Palaeogeography, Palaeoclimatology, Palaeoecology* **506**: 226–241.

Bazzicalupo, P., Maiorano, P., Girone, A., Marino, M., Combourieu-Nebout, N., Incarbona, A., 2020. High-frequency climate fluctuations over the last deglaciation in the Alboran Sea, western Mediterranean: evidence from calcareous plankton assemblages. *Palaeogeography, Palaeoclimatology, Palaeoecology* **506**, 226–241.

Bevington P.R., 1969. *Data Reduction and Error Analysis for the Physical Sciences*. McGraw Hill. New York, NY.

Bright, J., Ebert, C., Kosnik, M.A., Southon, J.R., Whitacre, K., Albano, P.G., Flores, C., *et al.*, 2021. Comparing direct carbonate and standard graphite ^{14}C determinations of biogenic carbonates. *Radiocarbon* **63**, 387–403.

Bush, S., Santos, Guaciara M., Xiaomei, X., Southon, J.R., Thiagarajan, N., Hines, S.K., Adkins, J.F., 2013. Simple, rapid, and cost effective: a screening method for ^{14}C analysis of small carbonate samples. *Radiocarbon* **55**, 631–640.

Cacho, I., Grimalt, J.O., Pelejero, C., Canals, M., Sierro, F.J., Flores, J.A., Shackleton, N., 1999. Dansgaard-Oeschger and Heinrich event imprints in Alboran Sea paleotemperatures. *Paleoceanography* **14**, 698–705.

Català, A., Cacho, I., Frigola, J., Pena, L.D., Lirer, F., 2019. Holocene hydrography evolution in the Alboran Sea: a multi-record and multi-proxy comparison. *Climate of the Past* **15**, 927–942.

Cheddadi, R., Lamb, H.F., Guiot, J., Van Der Kaars, S., 1998. Holocene climatic change in Morocco: a quantitative reconstruction from pollen data. *Climate Dynamics* **14**, 883–890.

Colonese, A.C., Mannino, M.A., Bar-Yosef Mayer, D.E., Fa, D.A., Finlayson, J.C., Lubell, D., Stiner, M.C., 2011. Marine mollusc exploitation in Mediterranean prehistory: an overview. *Quaternary International* **239**, 86–103.

Colonese, A.C., Troelstra, S., Ziveri, P., Martini, F., Lo Vetro, D., Tommasini, S., 2009. Mesolithic shellfish exploitation in SW Italy: seasonal evidence from the oxygen isotopic composition of *Osilinus turbinatus* shells. *Journal of Archaeological Science* **36**, 1935–1944.

Dettman, D.L., Reische, A.K., Lohmann, K.C., 1999. Controls on the stable isotope composition of seasonal growth bands in aragonitic fresh-water bivalves (Unionidae). *Geochimica et Cosmochimica Acta* **63**, 1049–1057.

Fürsich, F.T., Aberhan, M., 1990. Significance of time-averaging for palaeocommunity analysis. *Lethaia* **23**, 143–152.

Grossman, E.L., Ku, T.L., 1986. Oxygen and carbon isotope fractionation in biogenic aragonite: temperature effects. *Chemical Geology: Isotope Geoscience Section* **59**(C), 59–74.

Heaton, T.J., Köhler, P., Butzin, M., Bard, E., Reimer, R.W., Austin, W.E.N., Ramsey, C.B., *et al.*, 2020. Marine20—the marine radiocarbon age calibration curve (0–55,000 cal BP). *Radiocarbon* **62**, 779–820.

Hutterer, R., Linstädter, J., Eiwanger, J., Mikdad, A., 2014. Human manipulation of terrestrial gastropods in Neolithic culture groups of NE Morocco. *Quaternary International* **320**, 83–91.

Hutterer, R., Schröder, O., Linstädter, J. 2021. Food and ornament: use of shellfish at Ifri Oudadane, a Holocene settlement in NE Morocco. *African Archaeological Review* **38**, 73–94.

Kidwell, S.M., 1998. Time-averaging in the marine fossil record: overview of strategies and uncertainties. *Geobios* **30**, 977–995.

Kidwell, S.M., Best, M.M.R., Kaufman, D.S., 2005. Taphonomic trade-offs in tropical marine death assemblages: differential time averaging, shell loss, and probable bias in siliciclastic vs. carbonate facies. *Geology* **33**, 729–732.

Kidwell, S.M., Bosence, D.W.J., 1991. Taphonomy and time-averaging of marine shelly faunas. In: Alison, P.A., Briggs, D.E.G. (Eds.) *Taphonomy: Releasing the Data Locked in the Fossil Record*. New York: Plenum, pp. 115–209.

Koppel, B., Szabó, K., Moore, M.W., Morwood, M.J., 2016. Untangling time-averaging in shell middens: defining temporal units using amino acid racemisation. *Journal of Archaeological Science: Reports* **7**, 741–750.

Kowalewski, M., 1996. Time-averaging, overcompleteness, and the geological record. *Journal of Geology* **104**, 317–326.

Kowalewski, M., Casebolt, S., Hua, Q., Whitacre, K.E., Kaufman, D.S., Kosnik, M.A., 2018. One fossil record, multiple time resolutions: disparate time averaging of echinoids and mollusks on a Holocene carbonate platform. *Geology* **46**, 51–54.

Kowalewski, M., Goodfriend, G.A., Flessa, K.W., 1998. High-resolution estimates of temporal mixing within shell beds: the evils and virtues of time-averaging. *Paleobiology* **24**, 287–304.

Linstädter, J., Broich, M., Weninger, B., 2016. Defining the Early Neolithic of the Eastern Rif, Morocco—spatial distribution, chronological framework and impact of environmental changes. *Quaternary International* **472**, 272–282.

Linstädter, J., Kehl, M., 2012. The Holocene archaeological sequence and sedimentological processes at Ifri Oudadane, NE Morocco. *Journal of Archaeological Science* **39**, 3306–3323.

Linstädter, J., Wagner, G., 2013. The Early Neolithic pottery of Ifri Oudadane, NE Morocco—qualitative and quantitative evidence. *Journal of African Archaeology* **11**, 155–196.

Linstädter, J., Wagner, G., Broich, M., Gibaja Bao, J., Rodríguez, A.d.C., 2015. Neolithic transition and lithic technology: the Epipalaeolithic and Early Neolithic assemblages of Ifri Oudadane, NE-Morocco. *Quartär* **62**, 155–184.

Linstädter, J., 2008. The Epipalaeolithic-Neolithic-Transition in the Mediterranean region of Northwest-Africa. *Quartär* **55**, 41–62.

Lorenz, S.J., Lohmann, G., 2004. Acceleration technique for Milankovitch type forcing in a coupled atmosphere-ocean circulation model: method and application for the Holocene. *Climate Dynamics* **23**, 727–743.

Mannino, M., Thomas, K., Leng, M., Piperno, M., Tusa, S., Tagliacozzo, A., 2007. Marine resources in the Mesolithic and Neolithic at the Grotta dell'Uzzo (Sicily): evidence from isotope analyses of marine shells. *Archaeometry* **49**, 117–133.

Mannino, M.A., Thomas, K.D., Leng, M.J., Sloane, H.J., 2008. Shell growth and oxygen isotopes in the topshell *Osilinus turbinatus*: resolving past inshore sea surface temperatures. *Geo-Marine Letters* **28**, 309–325.

Martrat, B., Grimalt, J.O., Shackleton, N., Abreu, L.d., Hutterli, M.A., Stocker, T.A., 2007. Four climate cycles of recurring deep and surface water destabilizations on the Iberian margin. *Science* **27**, 502–507.

Mette, M.J., Whitney, N.M., Ballew, J., Wanamaker, A.D., 2018. Unexpected isotopic variability in biogenic aragonite: a user issue or proxy problem? *Chemical Geology* **483**, 286–294.

Michard, A., Saddiqi, O., Chalouan, A., Frizon de Lamotte, D., 2008. *Continental Evolution: The Geology of Morocco*. Springer-Verlag Berlin Heidelberg.

Milano, S., Prendergast, A.L., Schöne, B.R., 2016. Effects of cooking on mollusk shell structure and chemistry: Implications for archeology and paleoenvironmental reconstruction. *Journal of Archaeological Science: Reports* **7**, 14–26.

Milano, S., Lindauer, S., Prendergast, A.L., Hill, E.A., Hunt, C.O., Barker, G., Schone, B.R., 2018. Mollusk carbonate thermal behaviour and its implications in understanding prehistoric fire events in shell middens. *Journal of Archaeological Science: Reports* **20**, 443–457.

Morales, J., Pérez Jordà, G., Peña-Chocarro, L., Bokbot, Y., Vera, J.C., Martínez Sánchez, R.M., Linstädter, J., 2016. The introduction of southwestern Asian domesticated plants in north-western Africa: an archaeobotanical contribution from Neolithic Morocco. *Quaternary International* **412**, 96–109.

Morales, J., Pérez-Jordà, G., Peña-Chocarro, L., Zapata, L., Ruíz-Alonso, M., López-Sáez, J.A., Linstädter, J., 2013. The origins of agriculture in north-west Africa: macro-botanical remains from Epipalaeolithic and Early Neolithic levels of Ifri Oudadane (Morocco). *Journal of Archaeological Science* **40**, 2659–2669.

[NOAA] National Oceanic and Atmospheric Administration, 2012. Climate Prediction Center—North Atlantic Oscillation (NAO). http://www.cpc.ncep.noaa.gov/data/teledoc/nao.shtml.

New, E., Yanes, Y., Cameron, R.A.D., Miller, J.H., Teixeira, D., Kaufman, D.S., 2019. Aminochronology and time averaging of Quaternary land snail assemblages from colluvial deposits in the Madeira Archipelago, Portugal. *Quaternary Research* **92**, 483–496.

https://doi.org/10.1017/qua.2021.60 Published online by Cambridge University Press

Padgett, A., Yanes, Y., Lubell, D., Faber, M.L., 2019. Holocene cultural and climate shifts in NW Africa as inferred from stable isotopes of archeological land snail shells. *The Holocene* **29**, 1078–1093.

Parker, W., Yanes, Y., Mesa Hernández, E., Hernández Marrero, J.C., Pais, J., Surge, D., 2020. Scale of time-averaging in archaeological shell middens from the Canary Islands. *The Holocene* **30**, 258–271.

Parker, W., Yanes, Y., Mesa-Hernández, E., Surge, D., 2020. Oceanic cooling recorded in shells spanning the Medieval Climate Anomaly in the subtropical eastern North Atlantic Ocean. *Quaternary Science Reviews* **249**, 106635.

Parker, W., Yanes, Y., Surge, D., Mesa-Hernández, E., 2017. Calibration of the oxygen isotope ratios of the gastropods *Patella candei crenata* and *Phorcus atratus* as high-resolution paleothermometers from the subtropical eastern Atlantic Ocean. *Palaeogeography, Palaeoclimatology, Palaeoecology* **487**, 251–259.

Pierre, C., 1999. The oxygen and carbon isotope distribution in the Mediterranean water masses. *Marine Geology* **153**, 41–55.

Prendergast, A.L., Azzopardi, M., O'Connell, T.C., Hunt, C., Barker, G., Stevens, R.E., 2013. Oxygen isotopes from *Phorcus* (*Osilinus*) *turbinatus* shells as a proxy for sea surface temperature in the central Mediterranean: a case study from Malta. *Chemical Geology* **345**, 77–86.

Prendergast, A.L., Stevens, R.E., O'Connell, T.C., Fadlalak, A., Touati, M., Al-Mzeine, A., Schöne, B.R., Hunt, C.O., Barker, G., 2016. Changing patterns of eastern Mediterranean shellfish exploitation in the Late Glacial and Early Holocene: oxygen isotope evidence from gastropod in Epipaleolithic to Neolithic human occupation layers at the Haua Fteah cave, Libya. *Quaternary International* **407**, 80–93.

R Core Team, 2013. *R: A Language and Environment for Statistical Computing*. R Foundation for Statistical Computing, Vienna.

Reimer, P.J., McCormac, F.G., 2002. Marine radiocarbon reservoir corrections for the Mediterranean and Aegean Seas. *Radiocarbon* **44**, 159–166.

Shaltout, M., Omstedt, A., 2014. Recent sea surface temperature trends and future scenarios for the Mediterranean Sea. *Oceanologia* **56**, 411–443.

Siani, G., Paterne, M., Arnold, M., Bard, E., Métivier, B., Tisnerat, N., Bassinot, F., 2000. Radiocarbon reservoir ages in the Mediterranean Sea and Black Sea. *Radiocarbon* **42**, 271–280.

Stuiver, M., Braziunas T.F., 1993. Modeling atmospheric ^{14}C influences and ^{14}C ages of marine samples to 10,000 BC. *Radiocarbon* **35**, 137–189.

Stuiver, M., Polach, H.A., 1977. Reporting of ^{14}C data. *Radiocarbon* **19**, 355–363.

Stuiver, M., Reimer, P.J., Reimer, R.W., 2021. CALIB 8.2 (accessed January 20, 2021). http://calib.org.

Wanamaker, A.D., Jr., Kreutz, K.J., Schöne, B.R., Introne, D.S., 2011. Gulf of Maine shells reveal changes in seawater temperature seasonality during the Medieval Climate Anomaly and the Little Ice Age. *Palaeogeography, Palaeclimatology, Palaeoecology* **302**, 43–51.

Weisdorf, J.L., 2005. From foraging to farming: explaining the Neolithic Revolution. *Journal of Economic Surveys* **19**, 561–586.

Yanes, Y., Hutterer, R., Linstädter, J., 2018. On the transition from hunting-gathering to food production in NE Morocco as inferred from archeological *Phorcus turbinatus* shells. *The Holocene* **28**, 1301–1312.

Yanes, Y., Kowalewski, M., Ortiz, J.E., Castillo, C., Torres, T.d., Nuez, J.d.l., 2007. Scale and structure of time-averaging (age mixing) in terrestrial gastropod assemblages from Quaternary eolian deposits of the eastern Canary Islands. *Palaeogeography, Palaeoclimatology, Palaeoecology* **251**, 283–299.

Zapata, L., López-Sáez, J.A., Ruiz-Alonso, M., Linstädter, J., Pérez-Jordà, G., Morales, J., Kehl, M., Peña-Chocarro, L., 2013. Holocene environmental change and human impact in NE Morocco: palaeobotanical evidence from Ifri Oudadane. *The Holocene* **23**, 1286–1296.

Zilhão, J., 2014. Early prehistoric navigation in the western Mediterranean: implications for the Neolithic transition in Iberia and the Maghreb. *Eurasian Prehistory* **11**, 185–200.

https://doi.org/10.1017/qua.2021.60 Published online by Cambridge University Press